THE UNIVERSITY of EDINBURGH

Edinburgh Research Explorer

Murine gammaherpesvirus-68 infection causes multi-organ fibrosis and alters leukocyte trafficking in interferon-gamma receptor knockout mice

Citation for published version:
Ebrahimi, B, Dutia, BM, Brownstein, DG & Nash, AA 2001, 'Murine gammaherpesvirus-68 infection causes multi-organ fibrosis and alters leukocyte trafficking in interferon-gamma receptor knockout mice', *The American Journal of Pathology*, vol. 158, no. 6, pp. 2117-25. https://doi.org/10.1016/S0002-9440(10)64683-4

Digital Object Identifier (DOI):
10.1016/S0002-9440(10)64683-4

Link:
Link to publication record in Edinburgh Research Explorer

Document Version:
Publisher's PDF, also known as Version of record

Published In:
The American Journal of Pathology

Publisher Rights Statement:
© 2001 American Society for Investigative Pathology. Published by Elsevier Inc. All rights reserved.

General rights
Copyright for the publications made accessible via the Edinburgh Research Explorer is retained by the author(s) and / or other copyright owners and it is a condition of accessing these publications that users recognise and abide by the legal requirements associated with these rights.

Take down policy
The University of Edinburgh has made every reasonable effort to ensure that Edinburgh Research Explorer content complies with UK legislation. If you believe that the public display of this file breaches copyright please contact openaccess@ed.ac.uk providing details, and we will remove access to the work immediately and investigate your claim.

OPEN ACCESS

Download date: 05. May. 2023

American Journal of Pathology, Vol. 158, No. 6, June 2001
Copyright © American Society for Investigative Pathology

Murine Gammaherpesvirus-68 Infection Causes Multi-Organ Fibrosis and Alters Leukocyte Trafficking in Interferon-γ Receptor Knockout Mice

Bahram Ebrahimi, Bernadette M. Dutia, David G. Brownstein, and Anthony A. Nash

From the Laboratory for Clinical and Molecular Virology, Department of Veterinary Pathology, University of Edinburgh, Edinburgh, United Kingdom

Murine gammaherpesvirus-68 (MHV-68) infection in interferon-γ receptor knockout mice (IFN-γR$^{-/-}$) results in splenic fibrosis and excessive loss of splenocytes. In our present study we found that MHV-68 infection in IFN-γR$^{-/-}$ mice also resulted in fibrosis and atrophy of the mediastinal lymph nodes, interstitial pulmonary fibrosis and fibrotic changes in the liver. Atrophy and cellular depletion of the spleen in IFN-γR$^{-/-}$ was not the result of increased cell death. The loss of splenocytes in IFN-γR$^{-/-}$ mice, which was most evident on day 23 after infection, correlated with an increase in the number of leukocytes in peripheral blood. At the peak of leukocytosis, on day 23 after infection, peripheral blood cells from infected IFN-γR$^{-/-}$ mice were unable to traffic through the fibrosed spleens of IFN-γR$^{-/-}$ mice but were able to enter the spleens of wild-type mice. This indicates that leukocytosis was in part the result of emigration of cells from the spleen and their subsequent exclusion of re-entry at the height of fibrosis. Significant cytokine and chemokine changes were observed in spleens of IFN-γR$^{-/-}$ mice. IFN-γ, tumor necrosis factor-α (TNF-α), TNF-β, interleukin-1β (IL-1β), transforming growth factor-β1 (TGF-β1), lymphotactin, and MIP-1β were elevated on day 14 after infection whereas chemokines IP-10 and MIG were significantly reduced. These changes suggest a role for dysregulated cytokines and chemokines in severe organ-specific fibrosis with implications for immune-mediated fibrotic disorders. *(Am J Pathol 2001, 158:2117–2125)*

Murine gammaherpesvirus-68 (MHV-68) is a natural pathogen of murid rodents and is closely related to gammaherpesviruses Kaposi's sarcoma-associated herpesvirus, herpesvirus saimiri, and Epstein-Barr virus (EBV).[1] Infection of immunocompetent mice with MHV-68 via the respiratory route results in a lytic infection of alveolar epithelial cells and a latent infection in B cells.[2–3] Outcomes of the lytic phase of infection include a profound splenomegaly coincident with an increase of latently infected splenic B cells[4] and an infectious mononucleosis-like syndrome with an elevated Vβ4 CD8 T cell population.[5–6]

Interferon-γ is a key Th1 cytokine,[7] and it has been implicated in protective immune responses to several herpes viruses.[8–10] In herpes simplex virus-1 infection, lack of IFN-γ diminished the ability to clear the skin infection, with a delayed-type hypersensitivity response,[11,12] and infection in IFN-γR$^{-/-}$ mice with murine cytomegalovirus caused chronic aortic inflammation with prolonged shedding of infectious virus.[13]

IFN-γ is produced at high levels during the acute phase of MHV-68 infection,[14] and diminished levels of IFN-γ have been associated with recrudescence of lytic MHV-68 infection in lungs.[15,16] However, an unexpected outcome of MHV-68 infection in IFN-γR$^{-/-}$ mice via the respiratory route was severe splenic atrophy.[17] This observation demonstrated a novel function for this cytokine in maintaining the splenic architecture during a gammaherpesvirus infection.

The most striking feature of lymphoid pathology in IFN-γR$^{-/-}$ mice is splenic atrophy coupled with excessive deposition of collagen. The entire pathology is linked to the activity of CD8 T cells, because depletion of CD8 T cells resulted in maintenance of normal lymphoid architecture during the course of infection.[17]

Excessive collagen deposition in MHV-68-infected IFN-γR$^{-/-}$ mice would suggest a dysregulated cytokine response, because overexpression of cytokines IL-4, IL-1β, and TGF-β1, and reduced expression of interferon-γ have been shown to promote fibrosis[18,19] in, for example, systemic sclerosis[20,21] and murine models of fibrosis.[22,23]

In the present study we have identified hitherto unreported pathologies in the mediastinal lymph nodes, lungs, and liver and have further characterized the changes in the spleen of MHV-68-infected IFN-γR$^{-/-}$ mice. Moreover, we have explored possible mechanisms underlying spleen cell depletion and the pathological

Supported by grant 15/S009323 from the Biotechnology and Biological Sciences Research Council (UK).

Accepted for publication March 13, 2001.

Address reprint requests to Professor Anthony A. Nash, Department of Veterinary Pathology, University of Edinburgh, Summerhall, Edinburgh EH9 1QH, UK. E-mail: tony.nash@ed.ac.uk.

changes observed in these mice. Our data demonstrate that fibrosis and loss of splenocytes observed in IFN-$\gamma R^{-}/^{-}$ mice are associated with inhibition of leukocyte trafficking through the excessively fibrosed spleens of IFN-$\gamma R^{-}/^{-}$ mice, culminating in leukocytosis. Importantly, a dysregulated pattern of splenic cytokines and chemokines was observed in IFN-$\gamma R^{-}/^{-}$ mice, suggesting a possible explanation for the overt pathologies in IFN-$\gamma R^{-}/^{-}$ mice infected with MHV-68.

Materials and Methods

Mice

Adult wild-type (129/Sv/Ev) and IFN-$\gamma R^{-}/^{-}$ (129/Sv/Ev) mice were purchased from Bantin and Kingman (Hull, UK) and bred in-house.

Virus Infection and Sampling

MHV-68 virus stocks were prepared as previously described.[4] Mice (age- and sex-matched) were anesthetized with Halogen (Rhone Merieux Ltd., UK) and were inoculated via the intranasal route with 4×10^5 plaque-forming units of MHV-68 in 40 μl of sterile phosphate-buffered saline. At various time intervals, mice were sacrificed by CO_2 asphyxiation. Tissues were fixed in 10% buffered formal saline, paraffin-embedded, and 5-μm thick sections were stained with hematoxylin and eosin (H&E) and Masson's trichrome stain.

Death Assay

Terminal deoxynucleotide transferase-mediated dUTP nick end labeling (TUNEL) was performed on paraffin-embedded sections (*in situ* TUNEL) as previously described.[24]

Hematology and Flow Cytometry

Venous blood (inferior vena cava, 500 μl) was collected immediately at postmortem in EDTA tubes, stained with monoclonal antibodies against CD4 (YTS177.9.6.1), CD8 (YTS105.18.10), and CD19 (PharMingen), and analyzed on a FACStar Plus (Becton Dickinson) as previously described.[25] Total granulocyte counts were obtained from fluorescence-activated cell sorter profiles.

A Baker System 9100 hematology analyzer was used for hematological analyses. Differential white blood cell staining was carried out on a Bayer Hematek 2000 Stainer (Department of Veterinary Clinical Studies, Clinical Laboratory, Easter Bush Veterinary Center, Edinburgh, UK).

Leukocyte Trafficking

Peripheral blood was collected in EDTA tubes, and leukocytes were obtained by density centrifugation on Histopaque-1077 (Sigma). One milliliter of leukocytes (10^8/ml in diluent C) was mixed with one ml (10 μmol/L in diluent C) of green fluorescent dye PHK-67 (Sigma) for 6 minutes at room temperature with constant pipetting, followed by 2 ml of fetal calf serum and 4 ml of tissue culture medium Dulbecco's Modified Essential (DME) to terminate the labeling reaction. Labeled cells were centrifuged at low speed ($50 \times g$, three minutes) and resuspended in PBS. Each mouse was injected with 2×10^7/100 μl via the tail vein. Three mice were injected for each time point. After overnight injections, peripheral blood leukocytes (PBL) and splenocytes were obtained by density centrifugation. The presence of labeled cells was detected by FACS analysis of 200,000 events per each sample. The success of injection was based on the presence of labeled cells in PBL.

Ribonuclease Protection Assay

Ribonuclease protection assay (RPA) was used to quantitatively measure the expression of splenic cytokines and chemokines. Spleens were snap-frozen in liquid nitrogen immediately at postmortem and stored at −70°C before processing. Total RNA was isolated by RNAzolB solution (Biogenesis). Five micrograms of total RNA was hybridized to RPA probe sets: ML11 set (tumor necrosis factor-β, tumor necrosis factor-α, interleukin-4, IL-5, IL-1α, IFN-γ, IL-2, IL-6, IL-1β, IL-3, and L32), ML26 set (IL-3, IL-10, GM-CSF, TGF-β1, IL-13, IL-12p40, IL-12p35, IL-7, and L32), mCK5 set (LTN, RANTES, EOTAXIN, MIP-1β, MIP-1α, MIP-2, IP-10, MCP-1, TCA-3, L32, and glyceraldehyde-3-phosphate dehydrogenase (GAPDH); BD PharMingen; 45026P), and CCR7 set (IL-4, IL-12p40, IL-10, IL-1β, IL-13, CCR7, L32, and GAPDH; BD PharMingen; 557506). ML11 and ML26 sets were a kind gift from Dr. M. Hobbs, Scripps Research Institute, USA. The cloned murine monokine induced by interferon-γ (MIG) was a kind gift from Dr. M. Buchmeier (Scripps Research Institute). RPA assays were performed according to the RiboQuant protocol (BD PharMingen).

Bone Marrow Cellularity Measurement

Single cell suspensions of femoral bone marrow were prepared in RPMI 1640 [10% (v/v) fetal calf serum, 2 mmol/L glutamine, 100 U/ml penicillin and 100 μg/ml streptomycin] and cell numbers determined by hemocytometry.

Cytokine Protein Assays

Splenocytes were prepared by centrifugation over Ficoll-Hypaque (Histopaque 1077, Sigma), resuspended at 10^7 cells/ml in RPMI 1640 [10% (v/v) fetal calf serum, 2 mmol/L glutamine, 100 U/ml penicillin and 100 μg/ml streptomycin] and incubated at 37°C for 24 hours.[26] Supernatants were then harvested for enzyme-linked immunosorbent assays (ELISA). IFN-γ was measured using IFN-γ antibody pair (BD PharMingen) and according to the recommended protocol. TNF-α was assayed using

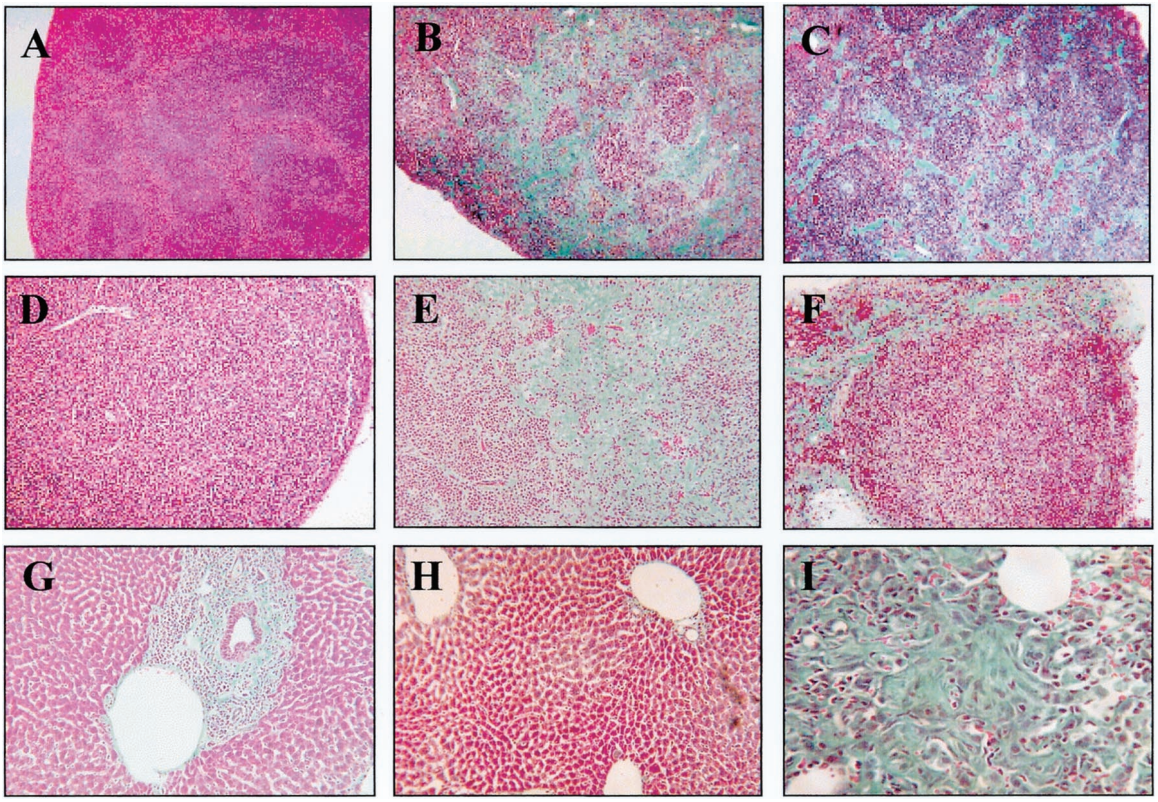

Figure 1. Pathological changes in IFN-$\gamma R^{-}/^{-}$ mice infected with MHV-68. Pathological changes on days 14 (**I**), 23 (**B**, **E**, and **G**), and 45 (**C**, **F**, and **H**) after infection with MHV-68. **A:** Normal spleen before infection. **B:** Fibrosis in sinusoids of red pulp. **C**: Partial resolution of fibrosis and contraction of residual fibrous tissue. **D:** Normal MLN before infection. **E:** Widespread fibrosis in MLN. **F:** Resolving fibrosis and increased cellularity in MLN. **G:** Periportal infiltrate encroaching on portal vein. **H:** Partial resolution of hepatic changes **I:** Interstitial pulmonary fibrosis. Sections **A** and **D** were stained with H&E, and sections **B**, **C**, and **E–I** were stained with Masson's trichrome. Representative sections are from five mice per each time point. Original magnifications: **A–F**, ×50; **G–H**, ×80; **I**, ×250.

the Quantikine M mouse TNF-α immunoassay kit (R&D Systems).

Results

To determine whether atrophy and fibrosis were confined to spleen and whether these changes were irreversible, we examined spleen, lymph nodes, lungs, and other major organs in wild-type and IFN-$\gamma R^{-}/^{-}$ mice at intervals up to 45 days after infection.

Histopathological Changes

The histological changes in spleens of wild-type and IFN-$\gamma R^{-}/^{-}$ mice were similar up to day 10, which included germinal centers and neutrophil infiltration of sinusoids. An apparent increase in neutrophils was noted in IFN-$\gamma R^{-}/^{-}$ mice. Extensive fibrosis was detected in spleens of IFN-$\gamma R^{-}/^{-}$ mice by day 23 after infection (all mice) with fibrosis in sinusoids and adjacent to germinal centers. Furthermore, spleens of IFN-$\gamma R^{-}/^{-}$ mice were significantly smaller than spleens of wild-type mice [130 mg $\pm$ 26.5 (SD) *versus* 31 $\pm$ 5.7, $P < 0.05$]. By day 45 after infection, spleens of IFN-$\gamma R^{-}/^{-}$ mice appeared more cellular compared to day 23, and showed signs of resolving pathology. In contrast, the spleens of wild-type mice maintained their normal architecture throughout the course of infection (Figure 1).

The patterns of pathology in mediastinal lymph node (MLN) were similar to the spleen in IFN-$\gamma R^{-}/^{-}$ mice. Initial changes (up to and including day 10) were similar in both wild-type and IFN-$\gamma R^{-}/^{-}$ mice (all mice), and consisted primarily of increased numbers of blast cells. By day 14, early fibrosis was observed in IFN-$\gamma R^{-}/^{-}$ mice, and by day 23, MLN in IFN-$\gamma R^{-}/^{-}$ mice showed signs of cellular depletion and atrophy. However, by day 45 we observed an increase in nodal cellularity with a partial resolution of scarring (Figure 1). Importantly, the pathological changes noted above were not observed in other secondary lymphoid tissues examined. For example, both the submandibular and the mesenteric lymph nodes in IFN-$\gamma R^{-}/^{-}$ mice appeared normal (data not shown).

The lymphoid tissues examined in the wild-type mice, similar to the spleens of these mice, maintained their normal architecture throughout the course of infection (data not shown).

Pathological changes were also noted in lungs and livers of IFN-$\gamma R^{-}/^{-}$ mice infected with MHV-68. The initial pulmonary changes were similar in both groups of mice by day 10 after infection. These changes included interstitial pneumonia and interstitial and intraalveolar fibrosis, accompanied by pulmonary phlebitis. The pulmonary

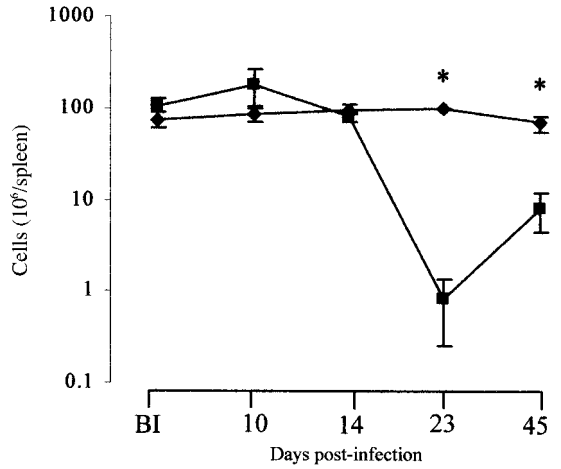

Figure 2. Splenic cellularity in MHV-68-infected mice. In contrast to wild-type mice, spleens of IFN-$\gamma R^{-}/^{-}$ mice were severely depleted by day 23 after infection but showed signs of partial repopulation by day 45 after infection. *, Significantly different from wild-type mice; $P < 0.05$. Numbers represent mean ± SD ($n = 3$). ♦, wild-type mice; ■, IFN-$\gamma R^{-}/^{-}$ mice.

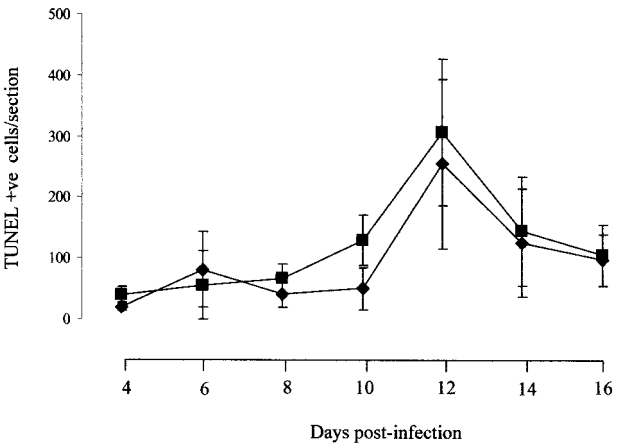

Figure 3. Apoptotic death in spleen. Spleens were fixed in formal saline and stained for TUNEL. All TUNEL-positive cells were counted on each section. Numbers of TUNEL-positive cells were comparable between IFN-$\gamma R^{-}/^{-}$ and wild-type mice during the course of infection. Numbers represent mean ± SD. ♦, wild-type mice; ■, IFN-$\gamma R^{-}/^{-}$ mice.

changes were most severe by day 14 after infection in IFN-$\gamma R^{-}/^{-}$ mice and included inflammation and interstitial fibrosis, accompanied by pulmonary phlebitis. The lungs also showed signs of resolution by day 45 after infection (Figure 1).

The hepatic changes in IFN-$\gamma R^{-}/^{-}$ mice were apparent on day 10 after infection and included multifocal dilation of sinusoids with fibrin deposits and infiltration by neutrophils and lymphocytes. Mild changes were observed in livers of wild-type mice, which included focal dilation of sinusoids with minor fibrin deposition and mixed inflammatory infiltrates (data not shown).

The mild pathological changes observed in the livers of wild-type mice were resolved by day 23 after infection (data not shown). In contrast, the hepatic changes in IFN-$\gamma R^{-}/^{-}$ mice had progressed from moderate to severe with extensive portal fibrosis. As with lymphoid tissue changes, most of hepatic changes had resolved by day 45 after infection (Figure 1).

Lymphoid Tissue Cellularity

To support the histological observations, we measured the cell numbers in lymphoid tissues during the course of infection. We found that by day 23 after infection, there was a 120-fold reduction in spleen cell numbers in IFN-$\gamma R^{-}/^{-}$ mice compared to wild-type mice [$9.7 \times 10^7 \pm 8.1 \times 10^5$ (SD) *versus* $8.1 \times 10^5 \pm 5.6 \times 10^5$, $P < 0.05$]. This reduction was followed by an increased cellularity of spleen in IFN-$\gamma R^{-}/^{-}$ mice evident by day 45 after infection [$8.1 \times 10^6 \pm 3.6 \times 0^6$ on day 45 *versus* $8.1 \times$] $10^5 \pm 5.6 \times 10^5$ on day 23, $P < 0.05$] (Figure 2). Similarly, the MLN of IFN-$\gamma R^{-}/^{-}$ mice were also depleted by day 23 after infection [$3.3 \times 10^6 \pm 6.4 \times 10^5$ (SD) *versus* $8 \times 10^4 \pm 1 \times 10^4$, $P < 0.05$].

Our histological observations indicated an apparent increase in neutrophils in IFN-$\gamma R^{-}/^{-}$ mice on day 10 after infection. This was also reflected in an increase in splenic neutrophils in IFN-$\gamma R^{-}/^{-}$ mice [17% ± 6.5 (SD) *versus* 13% ± 4.8].

Kinetics of Apoptotic Death in Spleen

The TUNEL assay was used to determine whether loss of splenocytes in IFN-$\gamma R^{-}/^{-}$ was due to increased apoptosis. The earliest TUNEL positive cells were detected on day 4 after infection, and were located in the periarterial lymphatic sheaths. From this point on, there was a gradual increase in numbers of TUNEL positive cells, which peaked at two weeks before a decline on day 16 after infection (Figure 3). At the peak of splenic apoptosis, the TUNEL positive cells were almost exclusively found within the follicular structures. However, both the tempo and the location of these TUNEL positive cells were similar in wild-type and IFN-$\gamma R^{-}/^{-}$ mice.

Hematological Changes

Lack of a substantial splenic apoptosis in IFN-$\gamma R^{-}/^{-}$ mice suggested the possibility of altered leukocyte trafficking, which could account for the loss of splenocytes in IFN-$\gamma R^{-}/^{-}$ mice. Therefore, we analyzed the hematological parameters in venous blood during the course of infection.

We found significant hematological changes in IFN-$\gamma R^{-}/^{-}$ mice which were apparent by day 10 after infection, where levels of circulating neutrophils were significantly elevated in comparison to those in wild-type mice (Figure 4).

By day 14 after infection, circulating leukocytes in IFN-$\gamma R^{-}/^{-}$ mice were, on average, greater than nearly threefold higher than those in the wild-type mice [$3.3 \times 10^7 \pm 1.2 \times 10^7$ (SD)/ml *versus* $1.3 \times 10^7 \pm 5 \times 10^6$, $P < 0.05$] and lymphocytes made as much as 78% of the rise in total white blood cells (Figure 4). The elevated circulating leukocytes in IFN-$\gamma R^{-}/^{-}$ mice reached a maximum on day 23 after infection [$3.5 \times 10^7 \pm 5.4 \times 10^6$ (SD)/ml

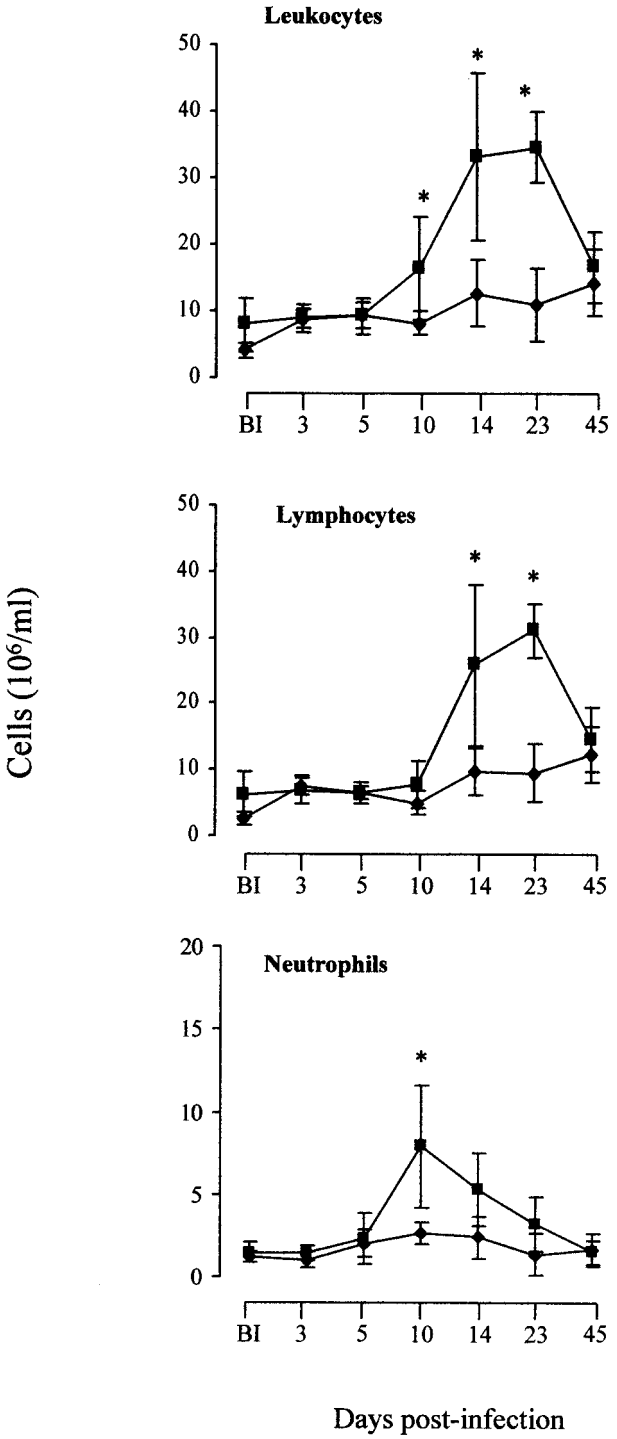

Figure 4. Hematological changes in MHV-68-infected mice. Venous blood was analyzed before infection and throughout the course of infection with MHV-68 BI. ◆, wild-type mice; ■, IFN-γR^{-}/$^{-}$ mice; *, significantly elevated in IFN-γR^{-}/$^{-}$ mice; $P < 0.05$. Numbers represent mean ± SD ($n = 5$).

versus $1.1 \times 10^7 \pm 5.4 \times 10^6$, $P < 0.05$]. Again, lymphocytes constituted the major population (89%) of circulating leukocytes (Figure 4).

The hematological changes observed at earlier time points in IFN-γR^{-}/$^{-}$ mice were resolved on day 45 after infection (Figure 4). At this late time point, the levels of circulating leukocytes in IFN-γR^{-}/$^{-}$ mice were more than

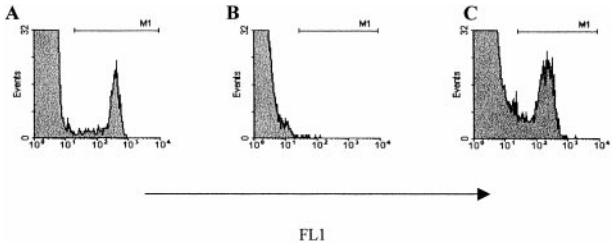

Figure 5. Inhibition of leukocyte trafficking through the severely fibrosed spleens. FACS analyses of splenocytes from (**A**) wild-type mice on day 23 after infection, (**B**) IFN-γR^{-}/$^{-}$ mice on day 23 after infection, and (**C**) IFN-γR^{-}/$^{-}$ mice on day 10 after infection injected 24 hours previously with labeled PBL from IFN-γR^{-}/$^{-}$ mice after 23 days after infection. Data are representatives of three mice per each group.

halved when compared to day 14, and were in the same range as circulating leukocytes in wild-type mice [$1.6 \times 10^7 \pm 5.3 \times 10^6$ (SD)/ml *versus* $1.4 \times 10^7 \pm 5 \times 10^6$] (Figure 4). These reductions in total venous blood leukocytes were similar to reductions in total lymphocyte levels [$1.4 \times 10^7 \pm 5 \times 10^6$ (SD)/ml *versus* $1.2 \times 10^7 \pm 4.3 \times 10^6$]. Notably, the resolution of leukocytosis also coincided with significant histological changes in spleens of IFN-γR^{-}/$^{-}$ mice (Figure 1).

We found no preferential expansion of any lymphocyte subset during leukocytosis. Moreover, the percentages of venous blood T (CD4 and CD8) and B (CD19) lymphocytes were similar between both wild-type and IFN-γR^{-}/$^{-}$ mice (data not shown). We also analyzed the femoral bone marrow cellularity in wild-type and IFN-γR^{-}/$^{-}$ mice. Bone marrow cellularity was comparable between wild-type and IFN-γR^{-}/$^{-}$ mice during the entire course of MHV-68 infection (data not shown).

Leukocyte Trafficking during MHV-68 Infection

To address the cause of leukocytosis, PBL from wild-type and IFN-γR^{-}/$^{-}$ mice were labeled with the green fluorescent dye, PKH-67, and used in cross transfer studies. PBL from IFN-γR^{-}/$^{-}$ mice (day 23 after infection) were able to traffic through the spleen of wild-type mice (day 23 after infection), but not through the spleens of IFN-γR^{-}/$^{-}$ mice on day 23 after infection (but did traffic through the spleens of these mice on day 10 after infection) (Figure 5). These data clearly show that an inhibition in cell trafficking between spleen and blood is a major cause of leukocytosis in IFN-γR^{-}/$^{-}$ mice.

Splenic Cytokine and Chemokine Changes

Multiprobe RPA sets and ELISA assays were used to analyze the levels of cytokines and chemokines, which may play a role in the pathologies observed in spleens of IFN-γR^{-}/$^{-}$ mice.

The splenic mRNA levels of IFN-γ were significantly higher in IFN-γR^{-}/$^{-}$ mice than in wild-type mice, reaching a peak on day 14 after infection [0.397 OD ± 0.018 (SD) *versus* 0.075 ± 0.018, $P < 0.05$]. Similarly, levels of TNF-α [0.683 OD ± 0.05 (SD) 0.3596 ± 0.06, $P < 0.05$], TNFβ [0.71 OD ± 0.17 (SD) *versus* 0.42 ± 0.12, $P < 0.05$], IL-1β [0.38 ± 0.03 OD (SD) *versus* 0.062 ± 0.01,

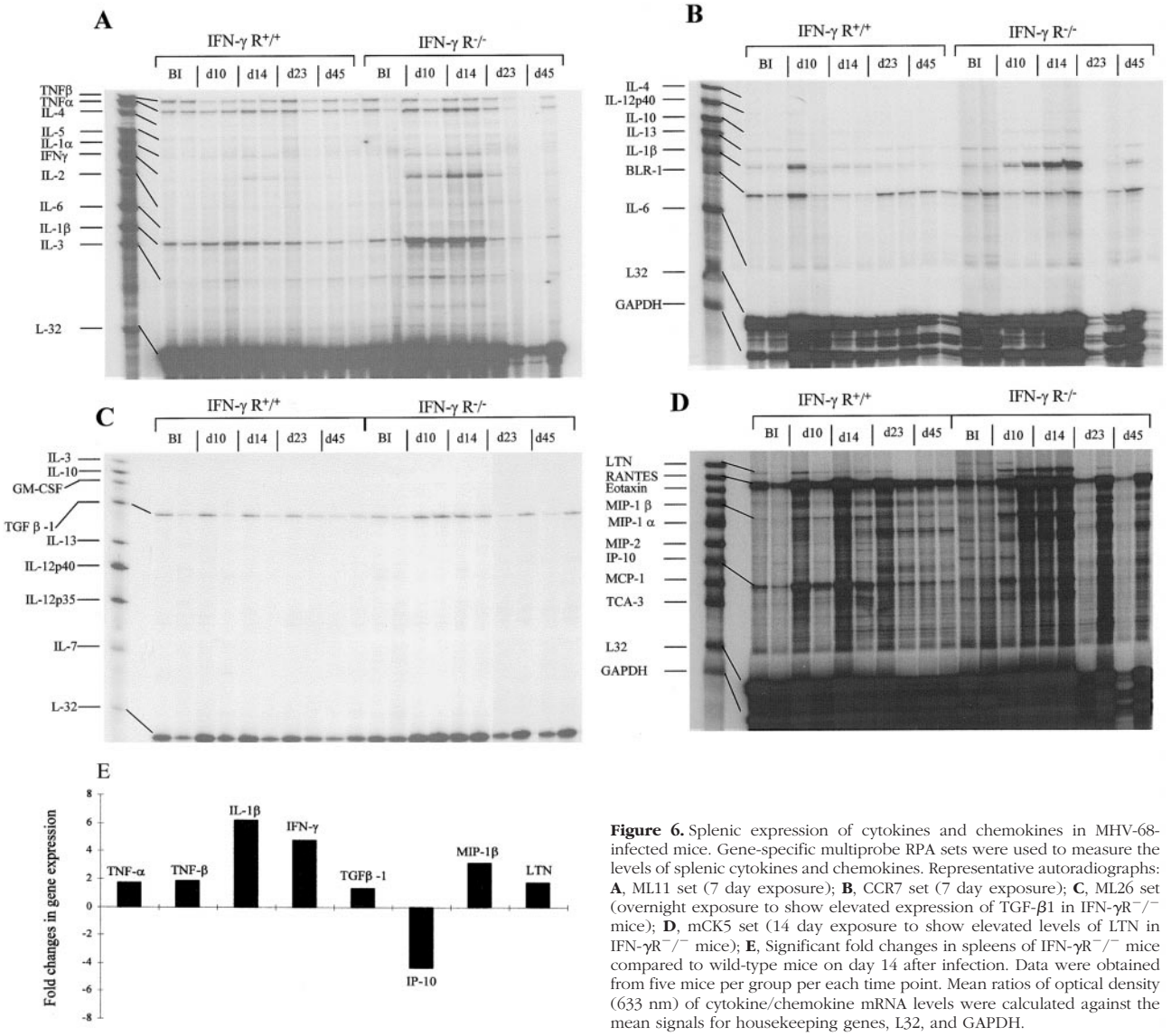

Figure 6. Splenic expression of cytokines and chemokines in MHV-68-infected mice. Gene-specific multiprobe RPA sets were used to measure the levels of splenic cytokines and chemokines. Representative autoradiographs: **A**, ML11 set (7 day exposure); **B**, CCR7 set (7 day exposure); **C**, ML26 set (overnight exposure to show elevated expression of TGF-β1 in IFN-$\gamma R^{-/-}$ mice); **D**, mCK5 set (14 day exposure to show elevated levels of LTN in IFN-$\gamma R^{-/-}$ mice); **E**, Significant fold changes in spleens of IFN-$\gamma R^{-/-}$ mice compared to wild-type mice on day 14 after infection. Data were obtained from five mice per group per each time point. Mean ratios of optical density (633 nm) of cytokine/chemokine mRNA levels were calculated against the mean signals for housekeeping genes, L32, and GAPDH.

$P < 0.05$], and TGF-β1 [3.17 ± 0.28 OD (SD) *versus* 2.44 ± 0.23, $P < 0.05$] were significantly elevated on day 14 after infection in spleens of IFN-$\gamma R^{-/-}$ mice compared to the wild-type mice (Figure 6).

The IFN-γ protein concentrations in splenocyte cultures from infected mice complemented the RPA data for this cytokine [32.075 ± 4.822 (SD) ng/ml *versus* 0.345 ± 0.466, $P < 0.05$]. Similarly, a TNF-α-specific ELISA was used to measure the protein concentration of this cytokine in splenocyte cultures obtained from infected mice. The splenic TNF-α protein levels were on average 2.8-fold higher in IFN-$\gamma R^{-/-}$ mice on day 14 after infection than in wild-type mice [0.536 ± 0.16 (SD) ng/ml *versus* 0.187 ± 0.057, $P < 0.05$] (Table 1).

In contrast to above, IP-10 was elevated in wild-type mice on day 14 after infection [0.322 ± 0.0432 (SD) OD *versus* 0.1033 ± 0.0163, $P < 0.05$] (Figure 6). Similarly, whereas the mRNA for MIG was readily detected in wild-type mice, we did not detect the transcript for this chemokine in IFN-$\gamma R^{-/-}$ mice (data not shown).

RANTES was abundantly expressed in both wild-type and IFN-$\gamma R^{-/-}$ mice. Interestingly, the elevated levels of this chemokine were sustained even at late time points when there was a reduction in other mRNA species studied (Figure 6).

Table 1. Cytokine Protein Concentrations in Splenocyte Cultures from MHV-68-Infected Mice

	Day	IFN-$\gamma R^{+/+}$	IFN-$\gamma R^{-/-}$
IFN-γ	10	3860 (3931)	12992 (±6060)
	14	345 (465)	32075 (±4821)*
TNF-α	10	276 (125)	273 (±82)
	14	187 (57)	536 (±159)*

Protein levels (pg/ml) were measured in supernatants of splenocytes cultured *in vitro* from MHV-68-infected mice. Note that in contrast to day 10, the levels of both cytokines were significantly elevated on day 14 in IFN-$\gamma R^{-/-}$ mice.

* Statistically elevated in IFN-$\gamma R^{-/-}$ mice; $P < 0.05$. Numbers represent mean ± SD ($n = 4$).

MIP1β levels were on average threefold higher on day 14 after infection in spleens of IFN-$\gamma R^{-}/^{-}$ mice than in wild-type mice [0.15 ± 0.08 (SD) *versus* 0.048 ± 0.02, $P < 0.05$] (Figure 6).

The basal levels of the chemokine lymphotactin were similar in both wild-type and IFN-$\gamma R^{-}/^{-}$ mice. However, the levels of this chemokine reached a peak on day 14 after infection and were significantly higher in IFN-$\gamma R^{-}/^{-}$ mice than in wild-type mice (0.12 ± 0.04 (SD) *versus* 0.07 ± 0.02, $P < 0.05$), before subsiding to pre-infection levels by day 45 after infection (Figure 6).

Discussion

Our findings show that MHV-68 infection of IFN-$\gamma R^{-}/^{-}$ mice results in fibrosis and atrophy of the spleen and MLN with severe cellular depletion of these organs culminating in leukocytosis. The pathologies in IFN-$\gamma R^{-}/^{-}$ mice include extensive mononuclear cell infiltration of the lung and the liver, with pulmonary interstitial fibrosis and hepatic portal fibrosis, respectively. The fibrosis and leukocytosis in IFN-$\gamma R^{-}/^{-}$ mice are associated with elevated levels of pro-fibrotic cytokines and a dysregulated chemokine response. These pathologies showed signs of resolution by day 45 after infection.

A prominent feature of splenic pathology in infected IFN-$\gamma R^{-}/^{-}$ mice is loss of splenocytes. Despite elevated levels of TNF-α and TNF-β in spleens of IFN-$\gamma R^{-}/^{-}$ mice, we found no significant increase in splenic apoptosis or changes in bone marrow cellularity to account for the reduced spleen cell numbers in these mice.

Our present work shows that the loss of splenic cellularity coincides with a dramatic increase in the number of T and B lymphocytes in peripheral blood. This is in agreement with our previous observation, in which T and B lymphocytes were lost from the spleens of IFN-$\gamma R^{-}/^{-}$ mice.[17] Furthermore, we found no particular increase in CD8 T cells during leukocytosis as observed in infectious mononucleosis seen in EBV and MHV-68.[5]

The increases in PBL in IFN-$\gamma R^{-}/^{-}$ mice were directly related to splenic atrophy, ie, the most depleted spleens had the highest levels of circulating leukocytes. This leukocytosis results, in part, from inhibited trafficking of peripheral blood cells through the fibrosed spleens of IFN-$\gamma R^{-}/^{-}$ mice. PBL taken from IFN-$\gamma R^{-}/^{-}$ mice at the height of leukocytosis (day 23) did not traffic through the spleens of IFN-$\gamma R^{-}/^{-}$ mice on day 23 after infection (ie, at the peak of leukocytosis), but were able to traffic through the spleens of wild-type mice synchronously infected with MHV-68 and also entered the spleens of IFN-$\gamma R^{-}/^{-}$ mice on day 10 after infection, ie, before extensive deposition of extracellular matrix.

We found that levels of IL-1β, TNF-α, TNF-β, TGF-β1, and IFN-γ were significantly elevated in spleens of IFN-$\gamma R^{-}/^{-}$ mice. Similar cytokine imbalances have also been associated with several human diseases with fibrosis and in murine models of fibrosis.[20–23] Of these cytokines, TNF-α, TGF-β1, and IL-1β are potent inducers of fibrosis,[27–28] whereas IFN-γ is a potent anti-fibrogenic cytokine and down-regulates the expression of both type I and type III collagens and fibronectin.[29–32] Consequently, lack of IFN-γ-mediated responses in IFN-$\gamma R^{-}/^{-}$ mice together with elevated levels of fibrogenic cytokines would further support a dysregulated cytokine response as a cause of fibrosis in IFN-$\gamma R^{-}/^{-}$ mice. Interestingly, a reduced trend in the expression of these cytokines coincided with a partial resolution of the pathologies by day 45 after infection. Moreover, despite the absence of a functional IFN-γ system, the cytokines IL-4 and IL-10, associated with Th2 responses were not upregulated in IFN-$\gamma R^{-}/^{-}$ mice.

The inhibited trafficking of leukocytes through the spleens of IFN-$\gamma R^{-}/^{-}$ mice prompted an analysis of chemokines, because they play a crucial role in leukocyte trafficking.[33] CXC chemokines IP-10 and MIG were significantly elevated in wild-type mice and are involved in the recruitment of T cells via the CXCR3 receptor.[34] Elevated levels of IP-10 and MIG were observed on day 14 after infection in infected wild-type mice (at the peak of splenomegaly), but were significantly reduced in the spleen of infected IFN-$\gamma R^{-}/^{-}$ mice (which lacked splenomegaly), further supporting previous observations on requirement of a functional IFN-γ for induction of these chemokines.[35] IP-10 has been shown to inhibit fibroplasia and deposition of extracellular matrix proteins,[36] and so a reduction in the expression of this chemokine and MIG during infection must affect splenic pathology.

MIP-1β and LTN are potent chemoattractants.[37] Paradoxically, spleens of IFN-$\gamma R^{-}/^{-}$ mice showed elevated levels of MIP-1β and LTN compared to wild-type mice. However, elevated levels of cytokines, for example TNFα, can inhibit cell migration by down-regulating chemokine receptors.[38] Therefore, a similar inhibitory mechanism may provide an explanation for the elevated levels of MIP-1β and LTN despite cellular depletion in IFN-$\gamma R^{-}/^{-}$ mice.

The pathologies associated with MHV-68 infection of IFN-$\gamma^{-}/^{-}$ mice may have important implications for human fibrotic conditions. Of significance here is the idiopathic pulmonary fibrosis (or cryptogenic fibrosing alveolitis), which is an immune-mediated disorder and has been associated with EBV infection.[39] Furthermore, several familial genetic defects associated with disruption of the IFN-γR have been reported in man.[40] Although no clinical viral disease has yet been identified in these patients, it is conceivable that a similar fate may ensue after infection with EBV or Kaposi's sarcoma-associated herpesvirus.

In conclusion, we demonstrated that MHV-68 initiates a cascade of pathological events in IFN-$\gamma R^{-}/^{-}$ mice. The expulsion of cells from the spleen leads to a rise in leukocytes in the peripheral blood. These cells are unable to re-enter the spleen despite, or because of, the elevated levels of inflammatory cytokines in the spleen. Tissue remodeling occurs, and there is a repopulation of the affected lymphoid tissues. Whereas data in this report may explain the likely molecular

basis for fibrosis, further work is needed to determine how MHV-68 gene expression alters the pattern of cytokines and chemokines in IFN-$\gamma R^{-}/^{-}$ mice and to understand the role of CD8 T cells in mediating this process.

Acknowledgment

We thank Heather Brooks for her excellent technical assistance and Neil MacIntyre for histology sections.

References

1. Speck SH, Virgin HW: Host and viral genetics of chronic infection: a mouse model of gamma-herpesvirus pathogenesis. Curr Opin Microbiol 1999, 2:403–409
2. Stewart JP, Usherwood EJ, Ross A, Dyson H, Nash T: Lung epithelial cells are a major site of murine gammaherpesvirus persistence. J Exp Med 1998, 187:1941–1951
3. Sunil-Chandra NP, Efstathiou S, Nash AA: Murine gammaherpesvirus 68 establishes a latent infection in mouse B lymphocytes in vivo. J Gen Virol 1992, 73:3275–3279
4. Sunil-Chandra NP, Efstathiou S, Arno J, Nash AA: Virological and pathological features of mice infected with murine gamma-herpesvirus 68. J Gen Virol 1992, 73:2347–2356
5. Tripp RA, Hamilton-Easton AM, Cardin RD, Nguyen P, Behm FG, Woodland DL, Doherty PC, Blackman MA: Pathogenesis of an infectious mononucleosis-like disease induced by a murine gamma-herpesvirus: role for a viral superantigen? J Exp Med 1997, 185:1641–1650
6. Flano E, Woodland DL, Blackman MA: Requirement for CD4+ T cells in V beta 4+CD8+ T cell activation associated with latent murine gammaherpesvirus infection. J Immunol 1999, 163:3403–3408
7. Boehm U, Klamp T, Groot M, Howard JC: Cellular responses to interferon-gamma. Annu Rev Immunol 1997, 15:749–795
8. Geginat G, Ruppert T, Hengel H, Holtappels R, Koszinowski UH: IFN-gamma is a prerequisite for optimal antigen processing of viral peptides in vivo. J Immunol 1997, 158:3303–3310
9. Orange JS, Wang B, Terhorst C, Biron CA: Requirement for natural killer cell-produced interferon gamma in defense against murine cytomegalovirus infection and enhancement of this defense pathway by interleukin 12 administration. J Exp Med 1995, 182:1045–1056
10. Bodaghi B, Goureau O, Zipeto D, Laurent L, Virelizier JL, Michelson S: Role of IFN-gamma-induced indoleamine 2,3 dioxygenase and inducible nitric oxide synthase in the replication of human cytomegalovirus in retinal pigment epithelial cells. J Immunol 1999, 162:957–964
11. Smith PM, Wolcott RM, Chervenak R, Jennings SR: Control of acute cutaneous herpes simplex virus infection: T cell-mediated viral clearance is dependent upon interferon-gamma (IFN-γ). Virology 1994, 202:76–88
12. Bouley DM, Kanangat S, Wire W, Rouse BT: Characterization of herpes simplex virus type-1 infection and herpetic stromal keratitis development in IFN-γ knockout mice. J Immunol 1995, 155:3964–3971
13. Presti RM, Pollock JL, Dal Canto AJ, O'Guin AK, Virgin HWT: Interferon gamma regulates acute and latent murine cytomegalovirus infection and chronic disease of the great vessels. J Exp Med 1998, 188:577–588
14. Sarawar SR, Cardin RD, Brooks JW, Mehrpooya M, Tripp RA, Doherty PC: Cytokine production in the immune response to murine gammaherpesvirus 68. J Virol 1996, 70:3264–3268
15. Cardin RD, Brooks JW, Sarawar SR, Doherty PC: Progressive loss of CD8+ T cell-mediated control of a gamma-herpesvirus in the absence of CD4+ T cells. J Exp Med 1996, 184:863–871
16. Christensen JP, Cardin RD, Branum KC, Doherty PC: CD4(+) T cell-mediated control of a gamma-herpesvirus in B cell-deficient mice is mediated by IFN-γ. Proc Natl Acad Sci USA 1999, 96: 5135–5140
17. Dutia BM, Clarke CJ, Allen DJ, Nash AA: Pathological changes in the spleens of gamma interferon receptor-deficient mice infected with murine gammaherpesvirus: a role for CD8 T cells. J Virol 1997, 71:4278–4283
18. Sempowski GD, Derdak S, Phipps RP: Interleukin-4 and interferon-gamma discordantly regulate collagen biosynthesis by functionally distinct lung fibroblast subsets. J Cell Physiol 1996, 167:290–296
19. Wallace WA, Ramage EA, Lamb D, Howie SE: A type 2 (Th2-like) pattern of immune response predominates in the pulmonary interstitium of patients with cryptogenic fibrosing alveolitis (CFA). Clin Exp Immunol 1995, 101:436–441
20. Atamas SP, Yurovsky VV, Wise R, Wigley FM, Goter Robinson CJ, Henry P, Alms WJ, White B: Production of type 2 cytokines by CD8+ lung cells is associated with greater decline in pulmonary function in patients with systemic sclerosis. Arthritis Rheum 1999, 42:1168–1178
21. Hunzelmann N, Anders S, Fierlbeck G, Hein R, Herrmann K, Albrecht M, Bell S, Thur J, Muche R, Adelmann-Grill B, Wehner-Caroli J, Gaus W, Krieg T: Systemic scleroderma: multicenter trial of 1 year of treatment with recombinant interferon gamma. Arch Dermatol 1997, 133:609–613
22. Baroni GS, D'Ambrosio L, Curto P, Casini A, Mancini R, Jezequel AM, Benedetti A: Interferon gamma decreases hepatic stellate cell activation and extracellular matrix deposition in rat liver fibrosis. Hepatology 1996, 23:1189–1199
23. Boros DL, Whitfield JR: Enhanced Th1 and dampened Th2 responses synergize to inhibit acute granulomatous and fibrotic responses in murine schistosomiasis mansoni. Infect Immun 1999, 67:1187–1193
24. Allsopp TE, Scallan MF, Williams A, Fazakerley JK: Virus infection induces neuronal apoptosis: a comparison with trophic factor withdrawal. Cell Death Differ 1998, 5:50–59
25. Ehtisham S, Sunil-Chandra NP, Nash AA: Pathogenesis of murine gammaherpesvirus infection in mice deficient in CD4 and CD8 T cells. J Virol 1993, 67:5247–5252
26. Cousens LP, Orange JS, Biron CA: Endogenous IL-2 contributes to T cell expansion and IFN-gamma production during lymphocytic choriomeningitis virus infection. J Immunol 1995, 155:5690–5699
27. Kahaleh MB, Smith EA, Soma Y, LeRoy EC: Effect of lymphotoxin and tumor necrosis factor on endothelial and connective tissue cell growth and function. Clin Immunol Immunopathol 1988, 49:261–272
28. Krane SM, Goldring MB: Potential role for interleukin-1 in fibrosis associated with chronic ambulatory peritoneal dialysis. Blood Purif 1988, 6:173–177
29. Amento EP, Bhan AK, McCullagh KG, Krane SM: Influences of gamma interferon on synovial fibroblast-like cells. Ia induction and inhibition of collagen synthesis. J Clin Invest 1985, 76:837–848
30. Clark JG, Dedon TF, Wayner EA, Carter WG: Effects of interferon-gamma on expression of cell surface receptors for collagen and deposition of newly synthesized collagen by cultured human lung fibroblasts. J Clin Invest 1989, 83:1505–1511
31. Granstein RD, Murphy GF, Margolis RJ, Byrne MH, Amento EP: Gamma-interferon inhibits collagen synthesis in vivo in the mouse. J Clin Invest 1987, 79:1254–1258
32. Hyde DM, Henderson TS, Giri SN, Tyler NK, Stovall MY: Effect of murine gamma interferon on the cellular responses to bleomycin in mice. Exp Lung Res 1988, 14:687–704
33. Warnock RA, Campbell JJ, Dorf ME, Matsuzawa A, McEvoy LM, Butcher EC: The role of chemokines in the microenvironmental control of T versus B cell arrest in Peyer's patch high endothelial venules. J Exp Med 2000, 191:77–88
34. Loetscher M, Gerber B, Loetscher P, Jones SA, Piali L, Clark-Lewis I, Baggiolini M, Moser B: Chemokine receptor specific for IP10 and mig: structure, function, and expression in activated T-lymphocytes. J Exp Med 1996, 184:963–969
35. Neumann B, Emmanuilidis K, Stadler M, Holzmann B: Distinct functions of interferon-gamma for chemokine expression in models of acute lung inflammation. Immunology 1998, 95:512–521

36. Keane MP, Belperio JA, Arenberg DA, Burdick MD, Xu ZJ, Xue YY, Strieter RM: IFN-gamma-inducible protein-10 attenuates bleomycin-induced pulmonary fibrosis via inhibition of angiogenesis. J Immunol 1999, 163(10):5686–5692
37. Mantovani A: The chemokine system: redundancy for robust outputs. Immunol Today 1999, 20:254–257
38. Hornung F, Scala G, Lenardo MJ: TNF-alpha-induced secretion of C-C chemokines modulates C-C chemokine receptor 5 expression onperipheral blood lymphocytes. J Immunol 2000, 164(12):6180–187
39. Egan JJ, Woodcock AA, Stewart JP: Viruses and idiopathic pulmonary fibrosis. Eur Respir J 1997, 10:1433–1437
40. Jouanguy E, Lamhamedi-Cherradi S, Lammas D, Dorman SE, Fondaneche MC, Dupuis S, Doffinger R, Altare F, Girdlestone J, Emile JF, Ducoulombier H, Edgar D, Clarke J, Oxelius VA, Brai M, Novelli V, Heyne K, Fischer A, Holland SM, Kumararatne DS, Schreiber RD, Casanova JL: A human IFNGR1 small deletion hotspot associated with dominant susceptibility to mycobacterial infection. Nat Genet 1999, 21:370–378